Disorder and demixing in bidisperse particle systems assembling bcc crystals ⊗

Jasmin J. Kennard [0]; H. Jonathan Zelaya Solano [0]; Caleb D. Biddulph [0]; Ryan C. Prager; Julia Dshemuchadse 2 0

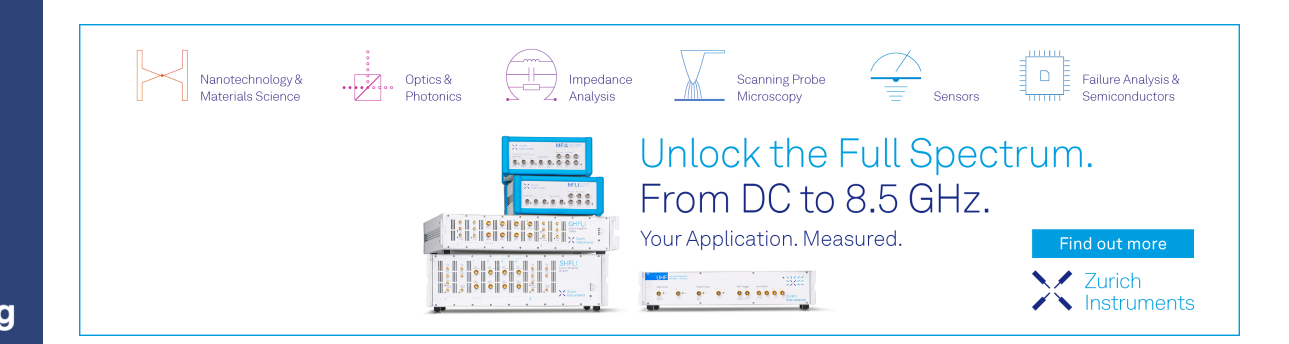


J. Chem. Phys. 161, 054715 (2024)

https://doi.org/10.1063/5.0219037









Disorder and demixing in bidisperse particle systems assembling bcc crystals

Cite as: J. Chem. Phys. 161, 054715 (2024); doi: 10.1063/5.0219037

Submitted: 14 May 2024 · Accepted: 15 July 2024 ·

Published Online: 7 August 2024







Jasmin J. Kennard, 1 D H. Jonathan Zelaya Solano, 2 D Caleb D. Biddulph, 3 D Ryan C. Prager, 2 and Julia Dshemuchadse^{2,a)}

AFFILIATIONS

- Robert F. Smith School of Chemical and Biomolecular Engineering, Cornell University, Ithaca, New York 14853, USA
- ²Department of Materials Science and Engineering, Cornell University, Ithaca, New York 14853, USA
- Department of Computer Science, Cornell University, Ithaca, New York 14853, USA

ABSTRACT

Colloidal and nanoparticle self-assembly enables the creation of ordered structures with a variety of electronic and photonic functionalities. The outcomes of the self-assembly processes used to synthesize such structures, however, strongly depend on the uniformity of the individual nanoparticles. Here, we explore the simplest form of particle size dispersity—bidispersity—and its impact on the self-assembly process. We investigate the robustness of self-assembling bcc-type crystals via isotropic interaction potentials in binary systems with increasingly disparate particle sizes by determining their terminal size ratio—the most extreme size ratio at which a mixed binary bcc crystal forms. Our findings show that two-well pair potentials produce bcc crystals that are more robust with respect to particle size ratio than one-well pair potentials. This suggests that an improved self-assembly process is accomplished with a second attractive length scale encoded in the particle-particle interaction, which stabilizes the second-nearest neighbor shell. In addition, we document qualitative differences in the process of ordering and disordering: in bidisperse systems of particles interacting via one-well potentials, we observe a breakdown of order prior to demixing, while in systems interacting via two-well potentials, demixing occurs first and bcc continues to form in parts of the droplet down to low size

Published under an exclusive license by AIP Publishing. https://doi.org/10.1063/5.0219037

INTRODUCTION

Colloidal and nanoparticle systems and their self-assembled ordered structures find increasing use in a variety of applications. Ordered assemblies of nanoparticles and colloids can exhibit tunable structural color, act as sacrificial templates in the "bottom-up" assembly of photonic crystals, 2,3 capture CO₂,4,5 and they can be used as sensors for humidity,6 glucose,7 and alcohol,8 and even to prepare catalysts.

The most basic model for studying thermodynamic phenomena in systems of mesoscopic particles such as crystallization is the hard-sphere model, featuring only excluded-volume interactions. This is often appropriate, as many colloidal dispersions such as polystyrene and silica particles largely behave as hard spheres. However, while many properties of colloidal systems can be represented through monodisperse spheres, size dispersity is practically inevitable in the nanoparticle synthesis process and has been observed to alter the freezing curve and crystallization kinetics of

colloidal systems. 10-12 The width of the size distribution of synthetic nanoparticles is rarely less than a few percent of their average radius, prompting considerable theoretical study of the phase behavior of polydisperse systems. 13-19 In addition to the breakdown of some crystallization behavior due to increasing size dispersity, recent computational studies have demonstrated the stabilization of AlB₂, Frank-Kasper, and Laves phases due to size dispersity.

Bidisperse systems, in which particles of only two different sizes are present in the system, constitute the simplest case of polydispersity and are consequently widely studied.²² ⁶ Binary systems have been shown to represent polydisperse fluids via bidisperse equivalent mapping, which proved useful over a range of compositions where one species does not dominate and over a wide range of volume fractions (except those near the jamming transition).²⁷ Several models for packing properties of mixtures designed for bidisperse systems were shown to be generalizable to polydisperse hard-sphere systems^{28,29} (and some studies have additionally examined the effect of both size and shape dispersity simultaneously³⁰).

a) Author to whom correspondence should be addressed: jd732@cornell.edu

While the hard-sphere model captures many features of self-assembling nanoparticle systems, explicit enthalpic interactions more closely model surface functionalizations that are typically applied to nanoparticles, making them effectively "soft." Softness has been shown to dramatically impact the self-assembled structures, and increased particle softness has been shown to stabilize the body-centered cubic (bcc) structure type in particular—as opposed to close-packed structures (face-centered cubic fcc/cubic close-packed ccp and hexagonal close-packed hcp)—in theoretical, $^{31-35}$ simulation, $^{36-40}$ and experimental studies. $^{41-49}$

The *bcc* structure type is one of the most prevalent crystal structure types among atomic elements (in, e.g., elemental iron, sodium, or tungsten),⁵⁰ and equivalent geometries are also commonly observed in colloidal and nanoparticle systems of spherical particles^{49,51–56} and systems of anisotropic particles.^{57,58} The *bcc* structure type has properties that make it superior to the closest sphere packings (i.e., *fcc/ccp* and *hcp*) on the atomic and nanoscale; for example, *bcc* is more resistant to deformation due to a high number of competing slip planes⁵⁹ and it often nucleates preferentially compared with other, lower-energy structures.⁶⁰ Numerous studies have observed *bcc* assemblies of nanoparticles in systems with variable polydispersities.^{61–64} Fractionation of constituents based on size has been observed experimentally in *bcc*-forming colloids with higher polydispersities around 0.14.¹⁹

To investigate the robustness of the assembly of *bcc*-forming systems, we simulate the self-assembly of particles that interact via isotropic pair potentials with one or two attractive wells.⁶⁵ These monodisperse systems exhibit a wide range of *bcc*-forming parameters, which we in turn use here to study these systems' behavior upon the introduction of size dispersity. We determine terminal size ratios between components in bidisperse systems and examine the mechanisms of structural breakdown. Specifically, we perturb the size of one component away from a known *bcc*-forming interaction potential and examine at what point *bcc* no longer forms. This provides novel insights into how likely these structures are to be observed experimentally in systems where particle dispersity is invariably present.

METHODS

Self-assembly simulations are conducted using the open-source simulation toolkit HOOMD-blue. 66,67 Molecular dynamics (MD) simulations are run in the canonical ensemble (NVT) using the Nosé–Hoover thermostat while enforcing periodic boundary conditions. Systems of N=4096 particles are initialized on a sparse grid in the gas phase at high temperature. Particles are randomly assigned velocities that are sampled from a Maxwell–Boltzmann distribution and randomly type-coded with the two different particle species, A and B.

We investigate the self-assembly behavior by performing cooling runs at linearly decreasing temperatures over 2×10^7 MD steps (with step size $\delta t = 0.005$). The starting temperature is chosen based on prior data such that the system condenses after $\sim 8 \times 10^6$ MD steps. (Condensation temperature data are included in the supplementary material.) Therefore, the systems can fully equilibrate in the liquid state prior to condensation; the end temperature of all simulations is set to kT = 0.1. Particles in all simulated systems

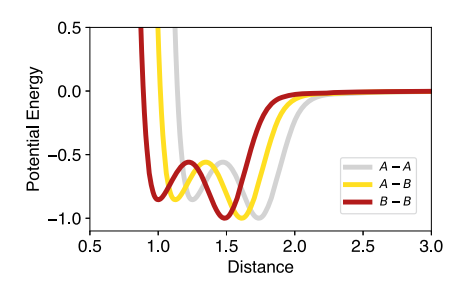


FIG. 1. Pairwise interactions between particles of types A and B with $r_0 = 1.5$, $\varepsilon = 1.0$, and s = 0.8. Potentials for A–A and A–B interactions are shifted to larger r values in accordance with Lorentz–Berthelot mixing rules.

condense into a liquid droplet and later either order into a crystalline structure or form an amorphous solid.

We model the interactions between particles with an isotropic pair interaction—the Lennard-Jones–Gauss (LJG) pair potential:

$$V_{\rm LJG}(r) = \frac{1}{(r-\Delta)^{12}} - \frac{2}{(r-\Delta)^6} - \varepsilon \exp\left(-\frac{(r-\Delta-r_0)^2}{2\sigma^2}\right),\,$$

if $r \leq 2.5$ and $V_{\rm LJG}(r)=0$ at larger interparticle distances beyond the radial cutoff $r > r_{\rm cutoff}=2.5$. The LJG pair potential is comprised of a Lennard-Jones potential with the addition of an attractive Gaussian. ^{68,69} Here, ε represents the depth and r_0 the radial position of the Gaussian well of each interaction. In this study, the well width is held constant at $\sigma^2=0.02$. The interaction potential is normalized such that the global minimum of the potential is -1: for ε values below 1.0, the Lennard-Jones well constitutes the global minimum of the interaction potential, while for ε values ≥ 1.0 , the Gaussian well is deepest.

The location of the minimum of the Lennard-Jones well of the pair potential corresponds to the effective diameter of each particle type (r_{AA} for the larger A-type particles and r_{BB} for the smaller B-type particles). We introduce particles of different sizes (see Fig. 1) via the Δ parameter:

- larger *A*-type particles interact via shifted LJG interactions: $\Delta_{AA} = r_{BB}/s r_{BB}$ for *A*-*A* interactions,
- smaller B-type particles interact via unshifted LJG interactions: Δ_{BB} = 0 for B–B interactions, and
- cross-interactions between larger and smaller particles are shifted halfway: $\Delta_{AB} = \frac{(r_{BB}/s r_{BB})}{2}$ for A-B interactions.

The characteristic size ratio of each binary particle system is $s = r_{BB}/r_{AA}$, and the interaction between unlike particles corresponds to an effective interparticle distance of $r_{AB} = (r_{AA} + r_{BB})/2$, in agreement with Lorentz–Berthelot mixing rules. ^{70,71} A comparison with other mixing rules is included in the supplementary material, showing no significant difference in the size-ratio dependence of the self-assembled structures and the terminal size ratio.

Particle mass is set such that the B-type particles all have a mass of 1.0 and the mass of the A-type particle is calculated such that both particle types exhibit the same density.

The parameter space of the potential is explored between $1 \le r_0 \le 2.1$ and $0 \le \varepsilon \le 5$ (position and depth of the Gaussian well, respectively) and for size ratios $0.5 \le s \le 1$. The lowest values of r_0 are chosen such that the position of the first attractive feature of the

pair potential corresponds to the Lennard-Jones well (as opposed to the Gaussian) for all state points. The maximum values of r_0 are chosen such that the interaction potential cutoff can be maintained and that $V(r_{\text{cutoff}} = 2.5 \cdot r_{ij}) \approx 0$ for all interactions $ij \in \{AA, AB, BB\}$.

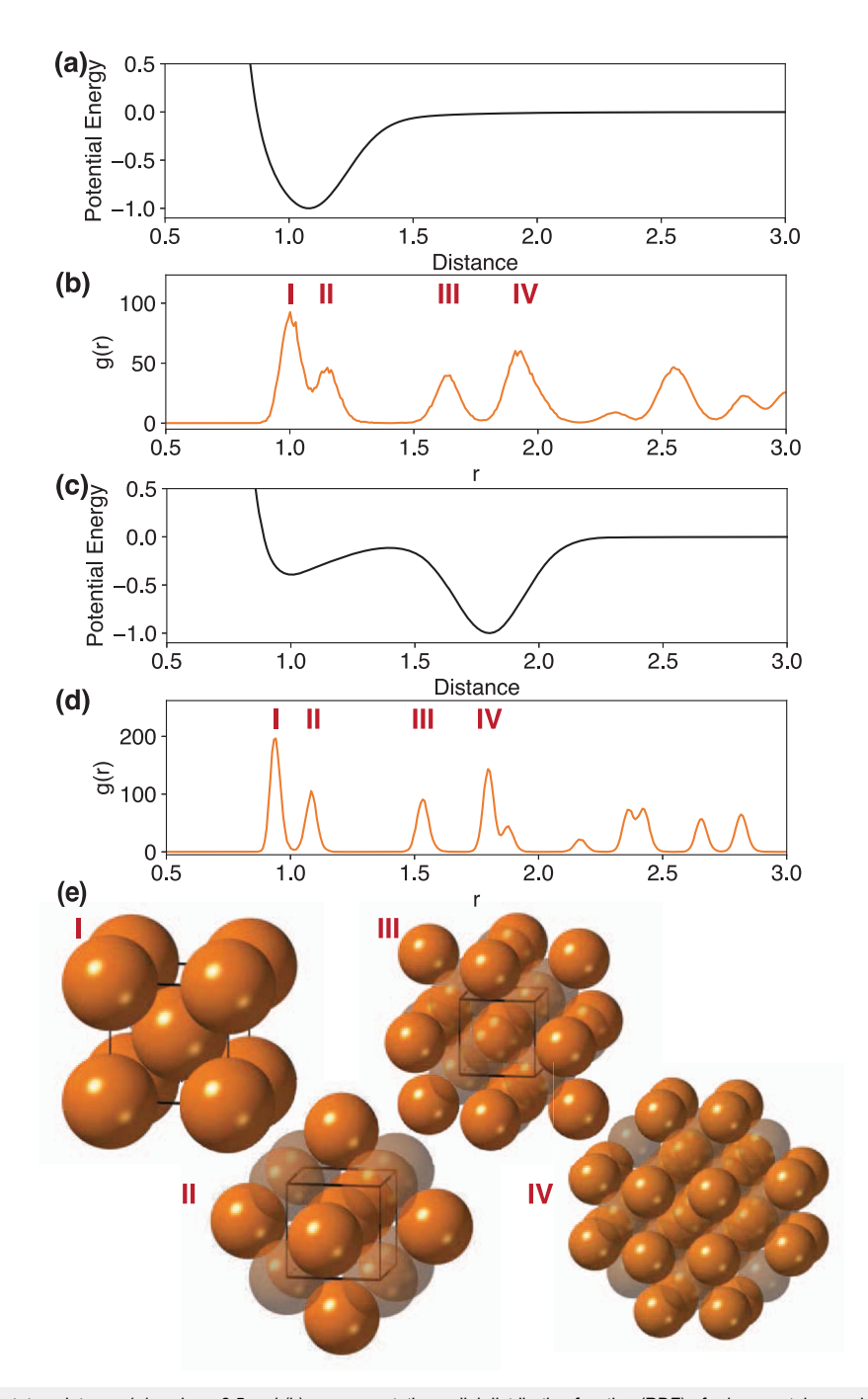


FIG. 2. (a) LJG potential for state point $r_0 = 1.1$ and $\varepsilon = 2.5$ and (b) a representative radial distribution function (RDF) of a *bcc* crystal comprised of particles interacting with that potential. (c) LJG potential for state point $r_0 = 1.8$ and $\varepsilon = 2.5$ and (d) a representative RDF of a *bcc* crystal comprised of particles interacting with that potential. (e) Nearest-neighbor arrangements corresponding to the peaks in the RDFs shown in (b) and (d).

All bidisperse, two-component systems are simulated at 1:1 compositions of *A*-to-*B*-type particles. A comparison of representative state points in each stability region at varying compositions is included in the supplementary material, showing that the composition did not substantially affect the terminal size ratio, only the number of particles in the crystalline solid. We attribute this behavior to the fact that the two components modeled in our systems are chemically similar and only differ in size, making them equivalent to metallic components that form solid solutions with wide stability regions, according to the Hume-Rothery rules.⁷²

In Fig. 2, we show example radial distribution functions (RDF) for two representative state points that form bcc ($r_0 = 1.1$ and $r_0 = 1.8$, both with $\varepsilon = 2.5$, corresponding to state points in the one-well and two-well stability regions, respectively). For ordered bcc-forming systems, the RDF exhibits narrow peaks corresponding to the distances of consecutive coordination shells in the crystal. For disordered systems, the RDF peaks are broader, and increasingly so at larger r values, due to the lack of long-range order. In systems where the components have demixed and both components still form bcc crystals, we expect to see a splitting of the nearest-neighbor peaks as A- and B-type particle sizes become more disparate.

Simulation trajectories are visualized with the Open Visualization Tool (OVITO),73 and crystal structures are visualized with CrystalMaker[®]. 74 Structures are determined using Common Neighbor Analysis (CNA),75 which analyzes the topology of each local particle environment and classifies it as bcc-, fcc-, hcp-type, icosahedral, or "other." The CNA parameter is used to determine the degree of bcc formation in each assembly as well as to determine terminal size ratios—that is, when bcc formation breaks down. In systems of N = 4096 particles, typically at most 3000 particles form the bulk of an assembly and adopt the bcc-type local environment, while the remaining particles are located at the surface and therefore have incomplete first-neighbor shells (which results in them being categorized as "other" by the CNA parameter). The first decrease in the number of bcc-type particles (below 3000) upon increasing the size difference of the A- and B-type particles is used to define the terminal size ratio. In this study, where particle assemblies are visualized or type-wise analysis is performed, A-type particles and their respective properties are shown in gray, B-type particles and their properties are shown in red, and cross-interactions between the two particle types are shown in orange.

We utilize the signac data management framework for computational workflow and data management. Data analysis, such as the calculation of RDFs, utilized the Freud library. Type-wise RDFs are calculated by separating the particles by type and considering only the neighbors of the second type listed around the particles of the first type listed, e.g., the A-B RDF only considers B-type neighbors around A-type particles.

RESULTS

One-component systems with shifted pair potentials

Prior to examining bidisperse systems—that is, mixtures of *A*-and *B*-type particles—we investigated pure systems of the larger, *A*-type particles with the aim of determining how the self-assembly

behavior is affected by a simple shifting of the interaction potentials. The self-assembly behavior of the smaller B-type particles had been studied previously, so we concentrated our study on state points at ε and r_0 values previously shown to form bcc-type structures. ⁶⁵ The bcc-forming state points are located in two distinct stability regions: around $r_0 = 1.1$ and $r_0 = 1.8$, as illustrated in Fig. 3. Because the r_0 values define the position of the Gaussian added to the Lennard-Jones well of the potential, and the LJ well is located at around r = 1, the stability region on the left (at smaller r_0 values) corresponds to a one-well pair potential, with the Gaussian distorting the shape of the LJ well [see Fig. 2(a)], while the stability region on the right (at larger r_0 values) corresponds to a two-well pair potential.

In Fig. 3, we represent the robustness of *bcc*-crystal formation with respect to the shift applied to the LJG potential to model A-type particles. The system's robustness is expressed via the effective particle size of the simulated A-type particles relative to the unshifted LJG potential—that is, the original effective particle size vs the simulated particle size $s = r_{BB}/r_{AA}$. Pure systems of A-type particles form bcc at effective particle sizes as low as s = 0.7, depending on their specific interaction potentials.

In the one-well potential region, state points appear most stable at $\varepsilon \leq 1$ and at higher values of r_0 , and they are moderately stable at $r_0 = 1.1$ —in the center of the stability region—across ε values. In the two-well potential region, state points appear most stable at higher values of r_0 and appear fairly insensitive to variation in ε . Globally, the one-well potential region contains some state points that are more stable than the two-well potential region.

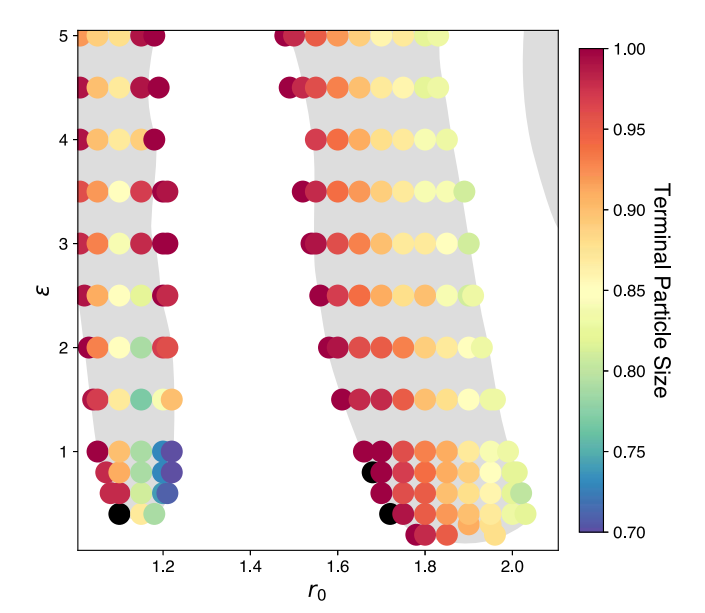


FIG. 3. *bcc* crystal formation in one-component systems of particles interacting via the shifted LJG potential. *bcc*-forming regions in unshifted pair potentials are denoted in gray background color. The robustness of each sampled state point to a shift of its interaction potential to higher values of *r* is indicated by its color, encoding the terminal particle size of *bcc*-formation (expressed through a ratio of the original effective particle size over the simulated particle size).

bcc-formation in bidisperse systems

The robustness of the crystallization in bidisperse systems was investigated in mixed systems of A- and B-type particles at 1:1 stoichiometry. Particles interacting via pair potentials corresponding to the two distinct stability regions located at $r_0 \approx 1.1$ and $r_0 \approx 1.8$ responded differently to the introduction of particle size bidispersity, as illustrated in Fig. 4 by their terminal size ratios. The reported terminal size ratio is the lowest size ratio at which a mixed, binary bcc structure forms across the entire condensed droplet in our self-assembly simulations.

When a second particle size is introduced in systems interacting via one-well pair potentials (at $r_0 \approx 1.1$), the bcc-type structure forms at size ratios close to 1, but as the size ratio between A- and B-type particles decreases below 0.95, only amorphous solids form. State points near and below $\varepsilon = 1$ are more robust with respect to the size ratio between A and B, indicating that larger deviations of the pair potential shape from a Lennard-Jones interaction lead to lower robustness with respect to size bidispersity—assemblies are more robust with respect to disparate particle sizes if the pair potential shape does not deviate significantly from the Lennard-Jones pair potential. Overall, the stability of bcc-formation decreases as ε increases, and at size ratios below the terminal size ratio, simulations form well-mixed amorphous clusters. The robustness of bcc assembly appears to be lower at high r_0 values in this region, if $\varepsilon > 1$. The mean terminal size ratio for state points sampled in the one-well

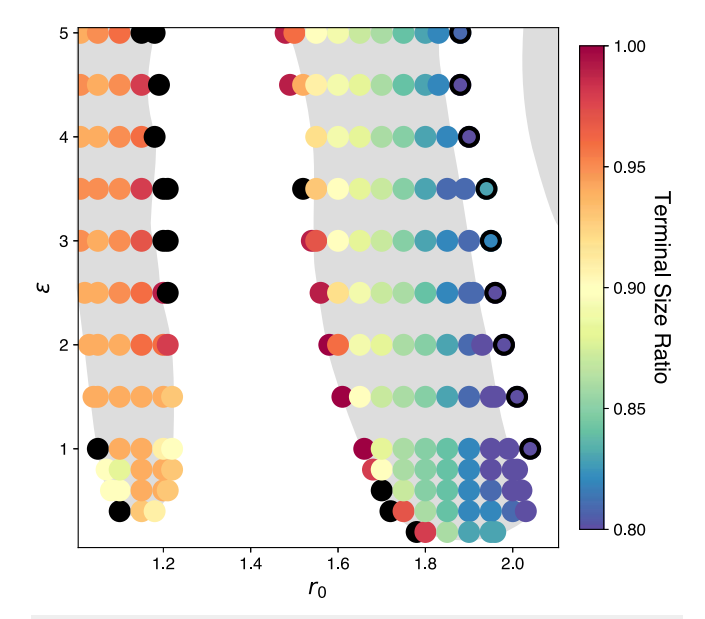


FIG. 4. *bcc* crystal formation in bidisperse systems of particles interacting via LJG potentials. *bcc*-forming regions are denoted in gray background color. The robustness of each sampled state point is indicated by its color, which encodes the terminal size ratio of *bcc* formation. The black-filled circles indicate state points that formed *bcc* on a longer time scale than the regions outlined in gray color, ⁵⁵ but which did not crystallize into *bcc* in this study, even in monodisperse systems, that is, s=1. State points beyond the right border of the two-well potential region are ringed in black, indicating that while a *bcc* crystal does not form at a size ratio of 1, reentrant behavior is observed at lower size ratios s<1.

potential region is 0.95 with a standard deviation of 0.03. This terminal size ratio corresponds to an effective terminal polydispersity of \sim 0.03. This contrasts with the results seen in several computational studies of *fcc*-forming systems of Lennard-Jones-type particles, which showed terminal polydispersities—the degree of size dispersity beyond which crystallization is suppressed—between 0.11 and 0.20. $^{18.79}$

In comparison to the one-well region, particles that interact with pair potentials from the two-well region located near $r_0 = 1.8$ appear to form bcc more robustly, with terminal size ratios generally below 0.90 except at the left boundary of the stability region (corresponding to the lowest r_0 values in this region). The mean terminal size ratio for state points sampled in the two-well potential region is 0.87 with a standard deviation of 0.06, corresponding to an effective terminal polydispersity of 0.07.

Two-well state points near and below $\varepsilon=1$ are also more robust with respect to the size ratio between A- and B-type particles. This aligns well with observations in systems of particles that interact with another isotropic pair potential—the oscillating pair potential: in the bcc stability region of the oscillating pair potential, we observed a similar trend, where the assembly process was most robust in systems in which the second well of the interaction potential was shallower than the first well (see supplementary material). In addition, the self-assembly behavior of particles in the double-well region is qualitatively very different: bcc-formation does not cease entirely in these simulations, but instead the systems demix more readily. This difference is evident when representative assemblies are investigated visually.

In Fig. 5, the number of *bcc*-type particles is plotted across varying size ratios for two representative state points, highlighting two distinct behaviors upon the introduction of bidispersity into these systems. Particles that interact via one-well pair potentials [Fig. 5(a)] exhibit an abrupt breakdown of crystallinity at their terminal size ratio: the number of *bcc*-type particles drops steeply from \sim 3000 to 0. In some cases—as shown in Fig. 5(a)—*bcc*-type particles reappear at very low size ratios, at which *A*- and *B*-type particles have demixed. Particles that interact via two-well pair potentials [Fig. 5(b)] exhibit a more gradual decrease in crystallinity: the smoother downturn of *bcc*-type particles, which corresponds to the size ratio at which demixing occurs.

The snapshots of representative state points from the one-well and the two-well interaction potential regions shown in Fig. 5 are colored both by particle type and by local structure. At high size ratios $s \approx 1$, where systems are essentially monodisperse, both stability regions show a single grain of *bcc* with clear faceting on the surface of the cluster and a thin layer of surface particles.

Particles that interact via one-well pair potentials exhibit a quicker disappearance of bcc-type order than those that interact via two-well pair potentials. In the narrow intermediate size-range regime, bcc still forms, but demixing starts to occur, and there is no visible faceting on the surface of the cluster. At lower size ratios, clusters are amorphous but still mixed; particles that interact with single-well pair potentials begin to demix only at even lower size ratios, for example, s = 0.7 in Fig. 5(a).

In the two-well region, shown in Fig. 5(b), the high size-ratio regime also forms clean, faceted *bcc*-type crystals. In the intermediate size-ratio regime, demixing occurs progressively toward lower

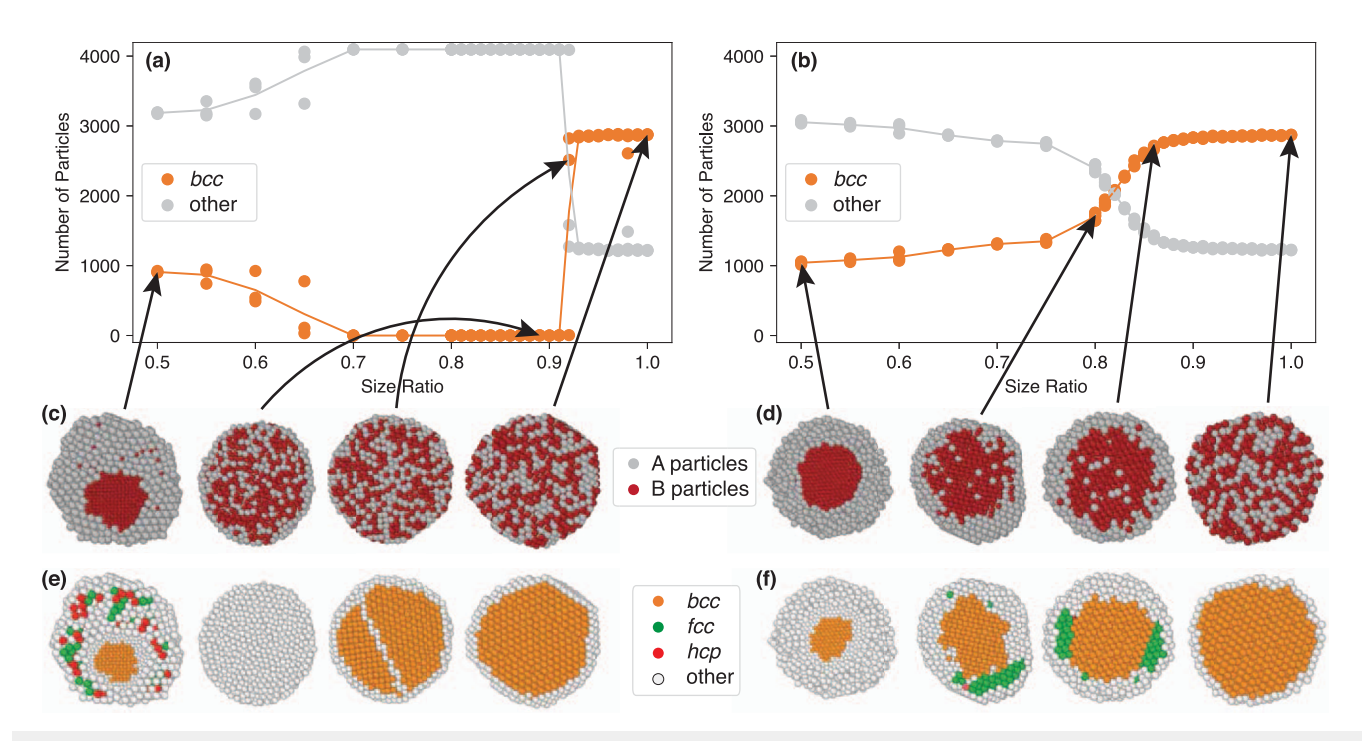


FIG. 5. Crystallinity and demixing behaviors in (a) the one-well pair potential region (state point $r_0 = 1.1$ and $\varepsilon = 2.5$) and (b) the two-well potential region (state point $r_0 = 1.8$ and $\varepsilon = 2.5$). At the top, the numbers of *bcc*-type particles at different size ratios are shown, demonstrating the breakdown behavior at particle size ratios below s = 1. Below, assembly cross-sections of different assemblies are shown with particles colored by type (c) for the one-well pair potential state point and (d) for the two-well pair potential state point, with *A*-type particles shown in gray and *B*-type particles in red. The same assembly cross-sections are shown with particles colored by local coordination environment—in (e) for the one-well pair potential and in (f) for the two-well pair potential state point—with orange representing *bcc*, green representing cubic close-packed (*ccp* or *fcc*), red representing hexagonal close-packed (*hcp*), and white representing all other coordination environments (including partially coordinated surface particles).

size ratios, where *bcc* dominates only in regions that are rich in *B*-type particles. As the degree of demixing increases, core-shell-type arrangements are formed: the core of these assemblies is made up of smaller *B*-type particles that exhibit a higher condensation temperature, while the outer shells are made up of larger *A*-type particles. At low size ratios, particle types are nearly completely demixed with the smaller particles forming a crystalline *bcc*-type core and the larger particles forming an outer shell that is often disordered. Alternatively, this outer shell can feature adjacent grains with *bcc*-type or other close-packed structures (*ccp/fcc* or *hcp*).

The structural transitions between ordered and (partially) disordered, as well as mixed and demixed assemblies, can be reviewed straightforwardly via the type-wise RDFs, as shown in Fig. 6. The breakdown in bcc crystallization is indicated by the blurring of the location of the neighbor shells, which occurs at relatively high size ratios for the one-well potential ($r_0 = 1.1$ state point: at s = 0.95) as opposed to much lower size ratios for the two-well potential ($r_0 = 1.8$ state point: at s = 0.81). The B-B RDF for the two-well pair potential shows sharp peaks across all size ratios in the B-B RDF [see Fig. 6(f)], indicating that B-type particles continue to form bcc.

The RDFs also illustrate the increase in the A-A and A-B nearest-neighbor distances as the size ratio decreases, while the effective A-type particle size increases. The B-B nearest-neighbor distance, however, differs between the systems of particles interacting via one- vs two-well pair potentials: the nearest-neighbor peak

for the one-well pair potential (with $r_0 = 1.1$) at size ratio s = 1 is located at r = 1.0 and the one for the two-well pair potential (with $r_0 = 1.8$) is located at r = 0.95 [see Figs. 6(c) and 6(f), as well as Fig. 2]. This indicates that systems whose particle-particle interactions exhibit similar first-well minima locations could form structures with different lattice parameters, effectively behaving as differently-sized particles, depending on their longer-range competing interactions, which here manifest as a second attractive well in the effective pair potential.

DISCUSSION

While polydispersity is a property that has been studied extensively in the field of nanoparticle synthesis, it is infrequently discussed or even reported in studies focusing on the mesoscale assembly of such particles, that is, in literature on the creation of so-called nanoparticle "superlattices." Furthermore, studies that report values for polydispersity vary considerably both in the determining method (small-angle X-ray scattering, transmission electron microscopy, dynamic light scattering, ultracentrifuge, and so on) and in the parameters used to represent polydispersity. Several systems formed mesoscale assemblies of *bcc* with reported polydispersities between 0.025 and 0.12^{49,61-64,80}—measured via the polydispersity index $PDI = \sigma_d/\bar{d}$, defined as the ratio of the standard deviation of

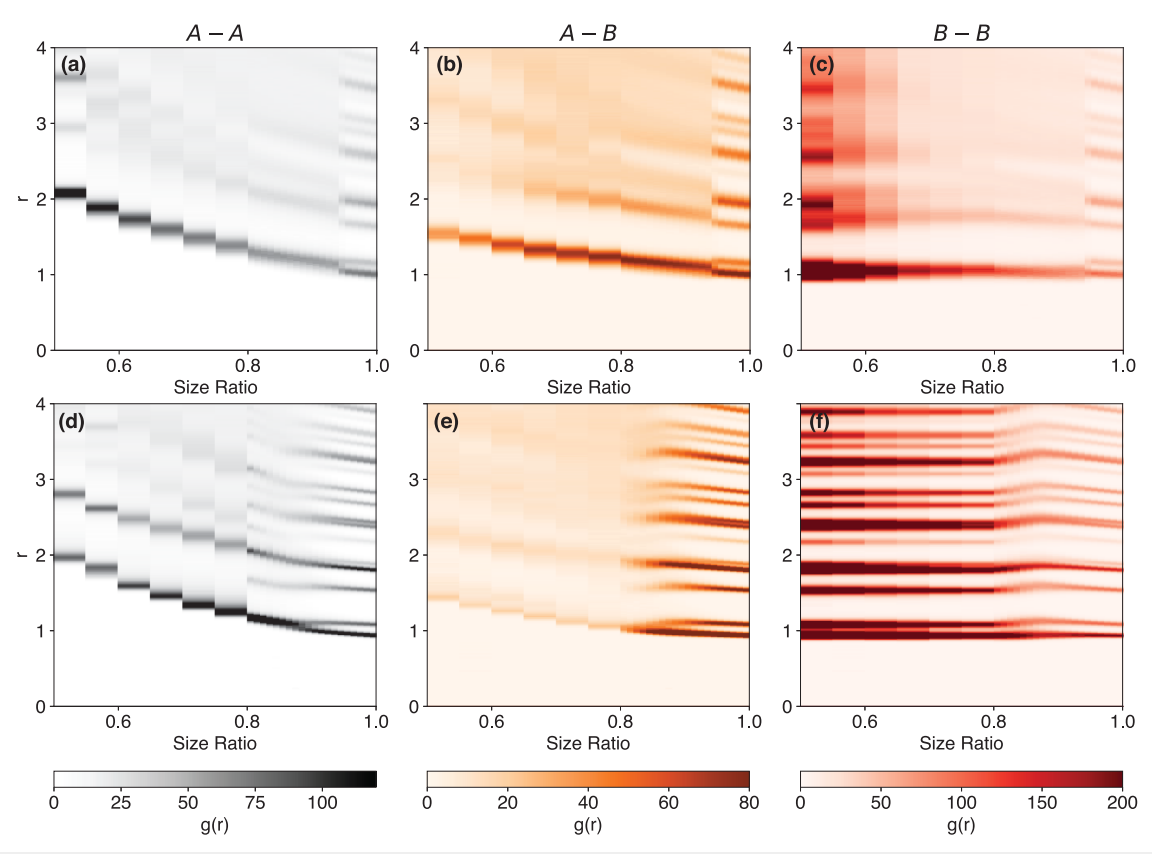


FIG. 6. Type-wise radial distribution functions (RDFs) for state points representing the (a)–(c) one-well (top) and (d)–(f) two-well pair potentials (bottom) ($r_0 = 1.1$, $\varepsilon = 2.5$ and $r_0 = 1.8$, $\varepsilon = 2.5$, respectively), illustrating coordinations between different pairs of particle types. A–A RDFs are depicted in gray, A–B RDFs are depicted in orange, and B–B RDFs are depicted in red. One-well pair potential RDFs: (a) A–A, (b) A–B, and (c) B–B. Two-well pair potential RDFs: (d) A–A, (e) A–B, and (f) B–B.

the particle diameter σ_d over the average diameter \bar{d} . These reported polydispersity values correspond to deviations in particle size consistent with our bidisperse systems with size ratios between s=0.94 and 0.79, that is, at similar values as the terminal size ratios determined here for bcc.

Self-assembly in monodisperse vs bidisperse systems

Self-assembly robustness in a one-component system does not appear to directly translate to self-assembly robustness in the corresponding two-component system. Even where both components reliably form bcc, a mixed system does not necessarily exhibit the same ordering behavior. For instance, the state point at $\varepsilon=1.0$ and $r_0=1.2$ has a terminal particle size of 0.70 in the monodisperse system but is more sensitive to size differences in the bidisperse system, at a terminal size ratio of 0.90. Similarly, for many larger-size particles where bcc does not form in the one-component system (with shifted pair potentials), we observe that the presence of the smaller-size, bcc-forming particles (with unshifted pair potentials) stabilizes the assembly of these particles in a mixed bcc-type crystal. This can be observed, for example, for the state point at $\varepsilon=1.0$ and $r_0=1.99$, which has a terminal particle size of 0.83 in the monodisperse sys-

tem but is somewhat more robust to particle size dispersity in the bidisperse system, with a terminal size ratio of 0.80.

The most robust region in the one-component system—below $\varepsilon=1.0$ and toward the right of the one-well stability region—is less robust than the majority of the two-well state points in the two-component system. No general trends could be found when comparing one- vs two-component systems, highlighting the non-trivial interactions that additional components contribute to system stability and self-assembly pathways.

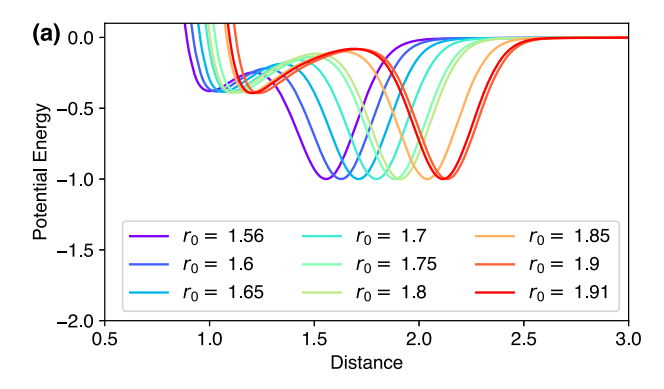
bcc crystals with different lattice parameters

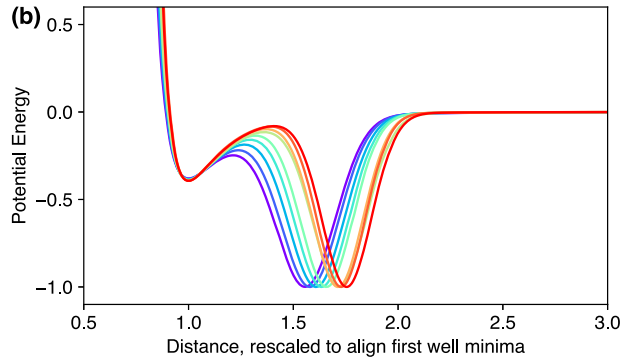
The different isotropic pair potentials investigated in this study all model particles that self-assemble *bcc* crystals—some with one-well and some with two-well functional forms. By mapping the positions of these attractive minima to the pairwise distances in the *bcc* crystal structure, we can understand how the resulting assemblies arise differently and how their response to particle size dispersity varies. The first four nearest-neighbor distances in a *bcc* crystal (see Fig. 2) are located at distances of approximately

$$r = d$$
, $\frac{2}{\sqrt{3}}d$, $2 \cdot \sqrt{\frac{2}{3}}d$, $\sqrt{\frac{11}{3}}d$,

with d denoting the nearest-neighbor distance between particles. The bcc-forming one-well pair potentials stabilize the first and second nearest-neighbor distances and the two-well pair potentials stabilize both the first- and second-nearest neighbors, as well as the third or fourth set of nearest neighbors.

The first and second nearest-neighbor distances combined form the first coordination shell of a particle in the bcc crystal structure—with 8+6=14 nearest neighbors. The third and fourth nearest-neighbor distances combined form the second coordination shell, which contains 12+24=36 nearest-neighbor particles. The fact that a greater number of neighbors sit in the more distant neighbor shells could result in the substantially higher stability





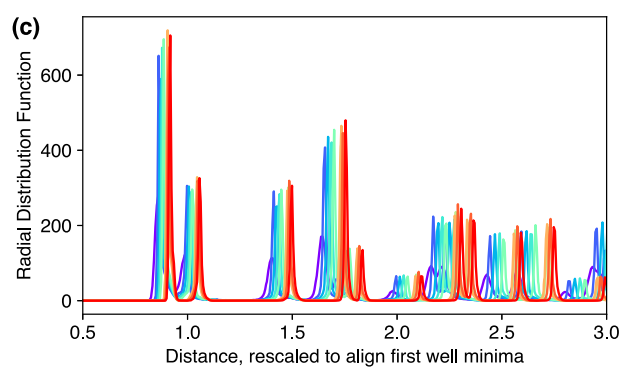


FIG. 7. Shifted LJG potentials of monodisperse assemblies, sampled at $\varepsilon=2.5$ in the two-well potential region. (a) Shifted potentials, plotted at maximal shifts at which *bcc* formation persists (terminal size ratio), (b) rescaled pair potentials with all first minima overlapping (at r=1.0), and (c) rescaled RDFs.

of assemblies in the two-well potential region compared with the one-well potential region, as seen in Fig. 4.

Because the first coordination shell of bcc is composed of two different nearest-neighbor distances as opposed to other close-packed structures (i.e., fcc/ccp and hcp, which exhibit 12 nearest neighbors at the same distance), either distance can potentially lie within the first minimum of the pair potential. The shifting of the first neighbor shell over r_0 suggests that the robustness of bcc formation in systems of particles that interact via two-well pair potentials is likely due to this added flexibility with respect to how the pair potential and the RDF of the resulting structure can align.

As the particle sizes become more disparate, the radial shift of the pair potential corresponding to the larger particles causes the relative distance between the first and second attractive minimum to decrease. This causes the pair potential to resemble a state point with lower r_0 —with slightly narrower wells. This is further supported by examining state points to the right of the bcc stability region, where we observe—at state points that do not form bcc at size ratio s=1.0—that bcc is self-assembled in bidisperse systems with size ratios just below 1 (see supplementary material). These size-shifted particles behave effectively as particles with lower r_0 values (within the bcc stability region) would.

In comparing the RDF and the interaction potential between particles (see Fig. 7), one can observe that the nearest-neighbor distance is not located exactly at the minimum of the first potential well of the two-well pair potential. Instead, the first- and second-nearest neighbors straddle the first minimum of the pair potential—the Lennard-Jones well-while the fourth nearest-neighbor distance matches the minimum of the second—Gaussian—well. This observation suggests that stabilization of more distant neighbor shells—in which more particles sit—is at least as important for assembly as stabilizing immediately adjacent particles. This agrees with recent experimental work demonstrating that increasing the electrical double-layer thickness of colloidal silica nanospheres through acid treatment enables their assembly into bcc crystals at low concentrations. 80 This motif of an increasing separation of the first and second attractive wells both energetically and in r—by the local maximum in the pair potential, which has its highest V(r) value at the largest r_0 parameters [see Fig. 7(b)]—also aligns with the location of the most stable parts of the self-assembly phase diagrams at the rightmost side of the bcc stability regions (see Figs. 3 and 4).

CONCLUSIONS AND OUTLOOK

In our study of a large number of isotropic pair potentials that self-assemble *bcc* crystals in simulation, we found that two-well pair potentials create assemblies that are much more robust to size dispersity—here mimicked via bidispersity—than one-well pair potentials, exhibiting terminal size ratios of 0.95 on average for one-well pair potentials vs 0.87 for two-well pair potentials. We posit that this is due to the second well in the pair potential stabilizing the nearest-neighbor distances of the second coordination shell in the *bcc* crystal structure, therefore inscribing the order of this simple structure onto the next-nearest neighbor coordination.

In addition, we found that the qualitative behavior of the *bcc* solid solution differs between one-well and two-well potentials. As the particle sizes become more disparate, particles interacting via one-well potentials experience a breakdown of crystalline order

prior to demixing, and particles interacting via two-well potentials demix while both components still form bcc crystals.

The terminal size ratios determined via self-assembly simulations corroborate the reported polydispersities at which nanoparticle assembly into ordered *bcc*-type structures is still observed in experimental studies. This indicates that our approximation of complex nanoparticle interactions in polydisperse systems with simple isotropic pair potentials in bidisperse systems in simulation is generally valid, rendering meaningful values for terminal polydispersities through computational means. We have shown that simple, chemistry-agnostic models can be used to derive meaningful semi-quantitative conclusions about crystallization phenomena, allowing simulations for future studies to be performed at larger scales than chemically-specific models due to our models' computational efficiency. This approach can therefore provide predictive analysis to guide future experimental studies of nanoparticle assemblies with non-closest-packed structures.

We find that the effective terminal polydispersities of these *bcc*-forming models are on average 0.03 and 0.07 for one- and two-well pair potential systems, both of which are distinctly smaller than the terminal polydispersities reported for *fcc*-forming Lennard-Jonestype particles. In the future, it will be interesting to investigate whether other crystal structures can be more robust to particle size dispersity than *fcc*. In future work, we hope to apply the herepresented methods to the self-assembly of other structures beyond the simple yet ubiquitous *bcc* crystals investigated here, in order to make predictions about the synthesizability of more diverse and complex structures formed by nanoparticles, en route to creating functional soft condensed materials.

SUPPLEMENTARY MATERIAL

The supplementary material includes data on systems of particles interacting with oscillating pair potentials, a comparison of different mixing rules, data on off-stoichiometric bidisperse systems, parameter scans in the LJG system, plots of the unscaled RDFs, nearest-neighbor distances in one-component systems of particles with size-shifted interaction potentials, a comparison of the features of the interaction potentials with the particle–particle distances in the formed crystals, data on the variation of the crystallization temperature, and data on the variation of the condensation temperature across state points.

ACKNOWLEDGMENTS

This material is based on work supported by the National Science Foundation under Grant No. DMR-2144094. Funding for this research was provided by the President's Council of Cornell Women (PCCW) Affinito-Stewart Grants Program. This work was performed using computational resources hosted at the Cornell University Center for Advanced Computing (CAC). We would also like to thank Hillary Pan, Maya M. Martirossyan, and Rachael S. Skye for helpful discussions.

AUTHOR DECLARATIONS

Conflict of Interest

The authors have no conflicts to disclose.

Author Contributions

Jasmin J. Kennard: Conceptualization (equal); Data curation (lead); Formal analysis (lead); Investigation (lead); Methodology (equal); Software (equal); Visualization (lead); Writing – original draft (lead); Writing – review & editing (equal). H. Jonathan Zelaya Solano: Investigation (supporting); Validation (lead); Writing – review & editing (supporting). Caleb D. Biddulph: Software (equal); Writing – review & editing (supporting). Ryan C. Prager: Software (equal); Writing – review & editing (supporting). Julia Dshemuchadse: Conceptualization (equal); Funding acquisition (lead); Methodology (equal); Project administration (lead); Resources (lead); Supervision (lead); Writing – original draft (supporting); Writing – review & editing (equal).

DATA AVAILABILITY

The data that support the findings of this study are openly available in Materials Data Facility 81 at http://doi.org/10.1063/5.0219037, Ref. No. 82.

REFERENCES

- ¹P. Liu, L. Bai, J. Yang, H. Gu, Q. Zhong, Z. Xie, and Z. Gu, Nanoscale Adv. 1, 1672 (2019).
- ²M. He, J. P. Gales, É. Ducrot, Z. Gong, G.-R. Yi, S. Sacanna, and D. J. Pine, Nature 585, 524 (2020).
- ³ A. Stein, B. E. Wilson, and S. G. Rudisill, Chem. Soc. Rev. 42, 2763 (2013).
- ⁴H. He, M. Zhong, D. Konkolewicz, K. Yacatto, T. Rappold, G. Sugar, N. E. David, J. Gelb, N. Kotwal, A. Merkle, and K. Matyjaszewski, Adv. Funct. Mater. **23**, 4720 (2013).
- ⁵ Y. Yang, L. Ohnoutek, S. Ajmal, X. Zheng, Y. Feng, K. Li, T. Wang, Y. Deng, Y. Liu, D. Xu, V. K. Valev, and L. Zhang, J. Mater. Chem. A 7, 11836 (2019).
- ⁶J. H. Kim, J. H. Moon, S.-Y. Lee, and J. Park, Appl. Phys. Lett. **97**, 103701 (2010).
 ⁷M. Ben-Moshe, V. L. Alexeev, and S. A. Asher, Anal. Chem. **78**, 5149 (2006).
- ⁸F. Wang, Z. Zhu, M. Xue, F. Xue, Q. Wang, Z. Meng, W. Lu, W. Chen, F. Qi, and Z. Yan, Sens. Actuators, B 220, 222 (2015).
- ⁹Y. Liu, L. Chen, T. Cheng, H. Guo, B. Sun, and Y. Wang, J. Power Sources 395, 66 (2018).
- $^{10}\text{S}.$ Martin, G. Bryant, and W. van Megen, Phys. Rev. E 67, 061405 (2003).
- ¹¹S. Martin, G. Bryant, and W. van Megen, Phys. Rev. E 71, 021404 (2005).
- H. J. Schöpe, G. Bryant, and W. van Megen, J. Chem. Phys. 127, 084505 (2007).
 R. P. Sear, Europhys. Lett. 44, 531 (1998).
- ¹⁴D. Coslovich, M. Ozawa, and L. Berthier, J. Phys.: Condens. Matter 30, 144004 (2018).
- ¹⁵B. A. Lindquist, R. B. Jadrich, and T. M. Truskett, J. Chem. Phys. **148**, 191101 (2018).
- ¹⁶P. Bartlett, J. Chem. Phys. **109**, 10970 (1998).
- ¹⁷P. N. Pusey, J. Phys. **48**, 709 (1987).
- ¹⁸Y. Terada, T. Keyes, J. Kim, and M. Tokuyama, AIP Conf. Proc. 1518, 776 (2013)
- ¹⁹R. Botet, B. Cabane, L. Goehring, J. Li, and F. Artzner, Faraday Discuss. 186, 229 (2016).
- ²⁰ P. K. Bommineni, N. R. Varela-Rosales, M. Klement, and M. Engel, Phys. Rev. Lett. **122**, 128005 (2019).
- ²¹B. Cabane, J. Li, F. Artzner, R. Botet, C. Labbez, G. Bareigts, M. Sztucki, and L. Goehring, Phys. Rev. Lett. 116, 208001 (2016).
- ²² E. V. Shevchenko, D. V. Talapin, C. B. Murray, and S. O'Brien, J. Am. Chem. Soc. 128, 3620 (2006).
- ²³E. Pretti, H. Zerze, M. Song, Y. Ding, N. A. Mahynski, H. W. Hatch, V. K. Shen, and J. Mittal, Soft Matter 14, 6303 (2018).

- ²⁴R. A. LaCour, T. C. Moore, and S. C. Glotzer, Phys. Rev. Lett. **128**, 188001 (2022).
- ²⁵ A. Travesset, Soft Matter **13**, 147 (2017).
- ²⁶H. Fang, M. F. Hagan, and W. B. Rogers, Proc. Natl. Acad. Sci. U. S. A. 117, 27927 (2020).
- ²⁷V. Ogarko and S. Luding, Soft Matter **9**, 9530 (2013).
- ²⁸L. Meng, P. Lu, and S. Li, <u>Particuology</u> **16**, 155 (2014).
- ²⁹C. Anzivino, M. Casiulis, T. Zhang, A. S. Moussa, S. Martiniani, and A. Zaccone, J. Chem. Phys. **158**, 044901 (2023).
- ³⁰ Y. Yuan, L. Liu, Y. Zhuang, W. Jin, and S. Li, Phys. Rev. E 98, 042903 (2018).
- ³¹ E. J. Meijer and F. El Azhar, J. Chem. Phys. **106**, 4678 (1997).
- ³²C. Rascón, E. Velasco, L. Mederos, and G. Navascués, J. Chem. Phys. **106**, 6689 (1997).
- ³³D. Gottwald, C. N. Likos, G. Kahl, and H. Löwen, Phys. Rev. Lett. **92**, 068301 (2004).
- ³⁴S. Prestipino, F. Saija, and P. V. Giaquinta, J. Chem. Phys. 123, 144110 (2005).
- ³⁵ A. Travesset, J. Chem. Phys. **141**, 164501 (2014).
- ³⁶K. Kremer, M. O. Robbins, and G. S. Grest, Phys. Rev. Lett. **57**, 2694 (1986).
- ³⁷M. O. Robbins, K. Kremer, and G. S. Grest, J. Chem. Phys. **88**, 3286 (1988).
- ³⁸ A.-P. Hynninen and M. Dijkstra, Phys. Rev. E **68**, 021407 (2003).
- ³⁹C. Desgranges and J. Delhommelle, J. Chem. Phys. **126**, 054501 (2007).
- ⁴⁰C. Desgranges and J. Delhommelle, J. Phys. Chem. B **111**, 12257 (2007).
- ⁴¹Y. Monovoukas and A. P. Gast, J. Colloid Interface Sci. 128, 533 (1989).
- ⁴²E. B. Sirota, H. D. Ou-Yang, S. K. Sinha, P. M. Chaikin, J. D. Axe, and Y. Fujii, Phys. Rev. Lett. **62**, 1524 (1989).
- ⁴³R. L. Whetten, M. N. Shafigullin, J. T. Khoury, T. G. Schaaff, I. Vezmar, M. M. Alvarez, and A. Wilkinson, Acc. Chem. Res. 32, 397 (1999).
- 44 B. A. Korgel and D. Fitzmaurice, Phys. Rev. B 59, 14191 (1999).
- ⁴⁵ A. Yethiraj and A. van Blaaderen, Nature **421**, 513 (2003).
- ⁴⁶B. W. Goodfellow and B. A. Korgel, ACS Nano 5, 2419 (2011).
- ⁴⁷ P. Tan, N. Xu, and L. Xu, Nat. Phys. **10**, 73 (2014).
- ⁴⁸R. V. Thaner, Y. Kim, T. I. N. G. Li, R. J. Macfarlane, S. T. Nguyen, M. Olvera de la Cruz, and C. A. Mirkin, Nano Lett. **15**, 5545 (2015).
- ⁴⁹B. W. Goodfellow, Y. Yu, C. A. Bosoy, D.-M. Smilgies, and B. A. Korgel, J. Phys. Chem. Lett. **6**, 2406 (2015).
- 50 W. Steurer, in *Physical Metallurgy*, 5th ed., edited by D. E. Laughlin and K. Hono (Elsevier, 2014), pp. 1–101.
- ⁵¹S. Lee, M. J. Bluemle, and F. S. Bates, Science **330**, 349 (2010).
- ⁵²R. J. Macfarlane, B. Lee, M. R. Jones, N. Harris, G. C. Schatz, and C. A. Mirkin, Science **334**, 204 (2011).
- ⁵³S. Chanpuriya, K. Kim, J. Zhang, S. Lee, A. Arora, K. D. Dorfman, K. T. Delaney, G. H. Fredrickson, and F. S. Bates, ACS Nano 10, 4961 (2016).
- ⁵⁴S. Lee, C. Leighton, and F. S. Bates, Proc. Natl. Acad. Sci. U. S. A. 111, 17723 (2014).
- ⁵⁵ K. Yue, M. Huang, R. L. Marson, J. He, J. Huang, Z. Zhou, J. Wang, C. Liu, X. Yan, K. Wu, Z. Guo, H. Liu, W. Zhang, P. Ni, C. Wesdemiotis, W.-B. Zhang, S. C. Glotzer, and S. Z. D. Cheng, Proc. Natl. Acad. Sci. U. S. A. 113, 14195 (2016).

- ⁵⁶S. A. Kim, K.-J. Jeong, A. Yethiraj, and M. K. Mahanthappa, Proc. Natl. Acad. Sci. U. S. A. 114, 4072 (2017).
- ⁵⁷J. Henzie, M. Grünwald, A. Widmer-Cooper, P. L. Geissler, and P. Yang, Nat. Mater. 11, 131 (2012).
- ⁵⁸ R. L. Marson, E. G. Teich, J. Dshemuchadse, S. C. Glotzer, and R. G. Larson, Soft Matter 15, 6288 (2019).
- ⁵⁹ H. Huh, K. Ahn, J. H. Lim, H. W. Kim, and L. J. Park, J. Mater. Process. Technol. 214, 1326 (2014).
- ⁶⁰S. Alexander and J. McTague, Phys. Rev. Lett. **41**, 702 (1978).
- ⁶¹ N. V. Dziomkina, M. A. Hempenius, and G. J. Vancso, Polymer **50**, 5713 (2009).
- 62 C. Zhou, J. Han, and R. Guo, J. Colloid Interface Sci. 397, 80 (2013).
- 63 T. Palberg, P. Wette, and D. M. Herlach, Phys. Rev. E 93, 022601 (2016).
- ⁶⁴H. J. Schöpe, T. Decker, and T. Palberg, J. Chem. Phys. **109**, 10068 (1998).
- ⁶⁵J. Dshemuchadse, P. F. Damasceno, C. L. Phillips, M. Engel, and S. C. Glotzer, Proc. Natl. Acad. Sci. U. S. A. 118, e2024034118 (2021).
- ⁶⁶J. A. Anderson, C. D. Lorenz, and A. Travesset, J. Comput. Phys. 227, 5342 (2008).
- ⁶⁷J. A. Anderson, J. Glaser, and S. C. Glotzer, Comput. Mater. Sci. **173**, 109363 (2020).
- ⁶⁸M. Rechtsman, F. Stillinger, and S. Torquato, Phys. Rev. E 73, 011406 (2006).
- ⁶⁹M. Engel and H.-R. Trebin, Phys. Rev. Lett. **98**, 225505 (2007).
- ⁷⁰H. A. Lorentz, Ann. Phys. **248**, 127 (1881).
- ⁷¹D. Berthelot, C. R. Acad. Sci. **126**, 1703 (1898), https://gallica.bnf.fr/ark:/ 12148/bpt6k3082d/f1703.
- ⁷²W. Hume-Rothery, Atomic Theory for Students of Metallurgy (The Institute of Metals, London, 1962).
- ⁷³ A. Stukowski, "Visualization and analysis of atomistic simulation data with OVITO-the Open Visualization Tool," Modell. Simul. Mater. Sci. Eng. 18, 015012 (2010).
- ⁷⁴D. Palmer, A. Fernandez, M. Gao, L. Rimmer, and E. Palmer, *CrystalMaker*[®], https://crystalmaker.com, 2024.
- ⁷⁵ A. Stukowski, Modell. Simul. Mater. Sci. Eng. **20**, 045021 (2012).
- ⁷⁶C. S. Adorf, P. M. Dodd, V. Ramasubramani, and S. C. Glotzer, Comput. Mater. Sci. 146, 220 (2018).
- ⁷⁷V. Ramasubramani, C. S. Adorf, P. M. Dodd, B. D. Dice, and S. C. Glotzer, in *Proceedings of the 17th Python in Science Conference* (SciPy, 2018), p. 152, http://doi.org/10.25080/Majora-4af1f417-016.
- ⁷⁸ V. Ramasubramani, B. D. Dice, E. S. Harper, M. P. Spellings, J. A. Anderson, and S. C. Glotzer, Comput. Phys. Commun. 254, 107275 (2020).
- ⁷⁹S. Sarkar, R. Biswas, M. Santra, and B. Bagchi, Phys. Rev. E **88**, 022104 (2013).
- ⁸⁰ Q. Fan, Z. Li, Y. Li, A. Gao, Y. Zhao, D. Yang, C. Zhu, T. V. Brinzari, G. Xu, L. Pan, L. T. Vuong, and Y. Yin, J. Am. Chem. Soc. 145, 28191 (2023).
- ⁸¹ B. Blaiszik, K. Chard, J. Pruyne, R. Ananthakrishnan, S. Tuecke, and I. Foster, "The materials data facility: Data services to advance materials science research," Met. Mater. Soc. 68, 2045 (2016).
- ⁸²J. J. Kennard, H. J. Zelaya Solano, C. D. Biddulph, R. C. Prager, and J. Dshemuchadse (2024). "Disorder and demixing in bidisperse particle systems assembling bcc crystals," Materials Data Facility, https://doi.org/10.18126/ts8g-1070.